Journal of Volcanology and Geothermal Research 302 (2015) 225–236

Contents lists available at ScienceDirect

Journal of Volcanology and Geothermal Research

journal homepage: www.elsevier.com/locate/jvolgeores

Heat flux from magmatic hydrothermal systems related to availability of fluid recharge

M.C. Harvey [a,*], J.V. Rowland [a], G. Chiodini [b], C.F. Rissmann [c], S. Bloomberg [d], P.A. Hernández [e,f], A. Mazot [g], F. Viveiros [h], C. Werner [i]

[a] School of Environment, University of Auckland, Auckland, New Zealand
[b] Istituto Nazionale di Geofisica e Vulcanologia sezione di Bologna"Osservatorio Vesuviano" Via Diocleziano, Napoli 328-80124, Italy
[c] Environment Southland, Private Bag 90116, Invercargill, New Zealand
[d] Department of Geological Sciences, University of Canterbury, Private Bag 4800, Canterbury, New Zealand
[e] Environmental Research Division, Instituto Tecnológico y de Energías Renovables (ITER), 38611 Granadilla de Abona, Spain
[f] Instituto Volcanológico de Canarias (INVOLCAN), 38400 Puerto de la Cruz, Spain
[g] GNS Science, Private Bag 2000, Taupo, New Zealand
[h] Centro de Vulcanologia e Avaliação de Riscos Geológicos, University of the Azores, Rua Mãe de Deus, Ponta Delgada 9501-801, Portugal
[i] Alaska Volcano Observatory, Volcano Science Center, U.S. Geological Survey, 4200 University Drive, Anchorage, AK 99508, USA

ARTICLE INFO

Article history:
Received 17 February 2015
Accepted 2 July 2015
Available online 15 July 2015

Keywords:
CO_2
Fumarole
Heat
Geothermal
Volcano
Energy

ABSTRACT

Magmatic hydrothermal systems are of increasing interest as a renewable energy source. Surface heat flux indicates system resource potential, and can be inferred from soil CO_2 flux measurements and fumarole gas chemistry. Here we compile and reanalyze results from previous CO_2 flux surveys worldwide to compare heat flux from a variety of magma-hydrothermal areas. We infer that availability of water to recharge magmatic hydrothermal systems is correlated with heat flux. Recharge availability is in turn governed by permeability, structure, lithology, rainfall, topography, and perhaps unsurprisingly, proximity to a large supply of water such as the ocean. The relationship between recharge and heat flux interpreted by this study is consistent with recent numerical modeling that relates hydrothermal system heat output to rainfall catchment area. This result highlights the importance of recharge as a consideration when evaluating hydrothermal systems for electricity generation, and the utility of CO_2 flux as a resource evaluation tool.

1. Introduction

A common model of a magmatic hydrothermal system consists of a convecting cell of fluid. Meteoric water exchanges heat with a magmatic body at depth then rises toward the surface through permeable rock formations as a high-temperature plume of low density water, steam and gas (mostly CO_2). Most of the rising steam condenses in the shallow subsurface, and the resulting liquid condensate is discharged from the system either by lateral outflow (Chiodini et al., 1996, 2005), or evaporation (Chiodini et al., 2005; Hochstein and Bromley, 2005; Werner et al., 2006). A proportion of the condensate may recycle back into the system through a "heat-pipe" mechanism (Hochstein and Bromley, 2005). Water discharged from the system (according to the above processes) is typically recharged at the margins by meteoric water (Giggenbach, 1995; Dempsey et al., 2012), or seawater in some coastal settings (Sveinbjornsdottir et al., 1986; Parello et al., 2000; Dotsika et al., 2009). In many systems, magmatic water is a minor component of recharge (Giggenbach, 1995). For most systems examined here, water is predominantly of meteoric origin. The quiescent-state heat flow from the system is useful for volcanic hazard monitoring, where a sudden increase in heat flow could precede a period of volcanic unrest. Heat flow evaluation is also useful for exploration of hydrothermal energy resources (Hochstein and Sudarman, 2008); magmatic hydrothermal systems are of increasing interest as low carbon sources of base load electricity (Chamorro et al., 2012).

When the CO_2/H_2O (unitless mass ratio) of the rising plume is known from fumarole gas analysis, and soil CO_2 flux can be quantified at the surface (using a portable CO_2 flux meter), the two can be combined to provide a proxy for heat flow, usually reported as megawatts (MW) (Brombach et al., 2001; Chiodini et al., 2005; Fridriksson et al., 2006; Hernández et al., 2012; Rissmann et al., 2012). The geostatistical methods used to quantify soil CO_2 flux were previously explored and compared (Lewicki et al., 2005). Accordingly, fumarole chemistry provides complementary information to CO_2 flux measurements (i.e. by allowing CO_2 flux to be used as a proxy for heat flow). However, in

* Corresponding author. Tel.: +64 21 1045 333.
E-mail address: mhar098@aucklanduni.ac.nz (M.C. Harvey).

http://dx.doi.org/10.1016/j.jvolgeores.2015.07.003

order to compare the intensity of heat flow from various volcanic and hydrothermal systems it is also useful to consider heat flux (MW/km^2), as distinct from heat flow (MW). Although the terms are often (erroneously) used interchangeably, heat flux is heat flow normalized to unit area (Bird et al., 1960).

Hydrothermal systems are generally characterized according to a number of factors including geochemistry (Giggenbach, 1996), reservoir phase (liquid or vapor), temperature, lithology, and structural setting (Henley and Ellis, 1983). Here we compile and reanalyze results from 22 hydrothermal areas representing a wide variety of settings. The objective is to determine how CO_2 flux, CO_2/H_2O and the associated heat flux vary according to structural setting, reservoir phase, recharge source and recharge availability. Refer to Table 1 for a detailed summary of the physical and chemical characteristics of these systems. Hydrothermal studies were included on the basis that they provided both system CO_2/H_2O, and mapping of the hydrothermal CO_2 flux and a total CO_2 flow, allowing an estimate of heat flow.

2. Methods

The data provided in Table 4 is used to construct Fig. 1. The data for 9 of the 22 systems in Table 4 comes from a previous study of CO_2 flux and fumarole analysis for a variety of hydrothermal systems (Chiodini et al., 2005). Our study expands the previous study with the addition of new systems, and by considering the relationship between system heat flux and system setting.

Where possible, we have adopted the methodology of the earlier study so additional systems can be included and meaningfully compared (refer to *Notes* in Tables 2 and 3 for exceptions). This methodology provides the mean soil diffuse CO_2 flux of diffuse degassing structures (DDS) present within the various systems. DDS correspond to discrete areas of anomalous CO_2 flux, commonly associated with areas of high permeability (faults). The methodology delineates DDS areas using sequential Gaussian simulation; for most surveys, DDS are defined as areas of anomalous CO_2 flux where simulated flux values

Table 1
System setting.

System	Heat flux	Recharge type[a]	Reservoir dominant phase[b]	Temperature[c]	Acid gases[d]	Fumarole chemistry[e]	Structural setting	Reference
Nisyros (all DDS), Greece	19–166	Magmatic (70%), seawater (30%)	Liquid	150–250, 300 (deep)	No	Mantle	Subduction	(Brombach et al., 2003; Dotsika et al., 2009)
Vesuvio Cone, Italy	55	Meteoric and magmatic	Vapor core	360+	No	Arc type – mar. carb.	Subduction	(Chiodini et al., 2001b, 2004)
Pantelleria, Fav Grande, Italy	69	Meteoric and/or seawater (≤30%)	Liquid	260	No	Mantle type	Extension	(Duchi et al., 1994; Parello et al., 2000; Gianelli and Grassi, 2001)
Latera, Italy	70	Meteoric	Liquid	210–230, ~340 (deep)	No	Arc	Subduction	(Chiodini et al., 2007)
Furnas, Azores archipelago, Portugal	95	Meteoric	Liquid	160–180	No	Mantle	Extension	(Cruz et al., 1999; Viveiros et al., 2010)
Masaya, Comalito, Nicaragua	97	Meteoric[f]	Vapor core	Unknown	Yes	Mantle + crust. carb.	Subduction	(Lewicki et al., 2003; Chiodini et al., 2005; MacNeil, 2006)
Solfatara (CF), Italy	118	Meteoric and magmatic	Vapor core	210–240 (vapor zone)	No	Arc	Subduction	(Panichi and Volpi, 1999; Chiodini et al., 2001a)
Yellowstone Mud V., USA	152	Ancient meteoric[a]	Vapor	300+ (deep)	Yes	Mantle	Hotspot	(Werner and Brantley, 2003; Rye and Truesdell, 2007; Werner et al., 2008b)
Vulcano, PL Beach, Italy	186	Meteoric and/or seawater and/or magmatic	Vapor core	230	No	Unknown	Island arc	(Bolognesi and D'Amore, 1993; Chiodini et al., 1995)
Vulcano Crater, Italy	193	Meteoric and/or seawater and/or magmatic	Vapor core	400+	Yes	Arc	Island arc	(Bolognesi and D'Amore, 1993; Chiodini et al., 1995)
White Island, New Zealand	205	Meteoric and seawater	Vapor core	600+	Yes	Arc	Island arc	(Giggenbach, 1987; Houghton and Nairn, 1991; Hedenquist et al., 1993; Giggenbach et al., 2003)
Yellowstone HSB, USA	211	Ancient meteoric[a]	Vapor	300+ (deep)	Yes	Mantle	Hotspot	(Werner and Brantley, 2003; Rye and Truesdell, 2007; Werner et al., 2008b)
El Tizate, Nicaragua	333	Meteoric	Liquid	250–285	Unknown	Unknown	Extensional	(Ostapenko et al., 1998)
Ohaaki West, New Zealand	343	Meteoric (86%), magmatic (14%)	Liquid	300	No	Arc	Extensional	(Giggenbach, 1995; Dempsey et al., 2012)
Yellowstone (HLGB), USA	352	Meteoric[a]	Liquid	200	No	Mantle	Hotspot	(Sheppard et al., 1992; Lowenstern et al., 2012)
Krafla, Iceland	425	Meteoric	Vapor core	190–210 300–350 (deep)	No	Mantle	Extensional	(Sveinbjornsdottir et al., 1986; Nielsen et al., 2000)
Rotokawa, New Zealand	427	Meteoric (92%), magmatic (8%)[a]	Liquid	320	Yes	Arc	Extensional	(Giggenbach, 1995; Dempsey et al., 2012)
Karapiti, Wairakei, New Zealand	432	Meteoric (92%), magmatic (8%)	Liquid (vapor shallow)	260	No	Mantle	Extensional	(Giggenbach, 1995; Glover and Mroczek, 2009; Dempsey et al., 2012)
Ischia, Donna Rachele, Italy	766	Meteoric and seawater[g]	Liquid	250 (shallow) 300 (deep)	No	Mantle	Island arc	(Inguaggiato et al., 2000; Chiodini et al., 2004; Chiodini et al., 2005)
Reykjanes, Iceland	1048	Seawater[a]	Liquid	290	No	Mantle	Extensional	(Sveinbjornsdottir et al., 1986; Fridriksson et al., 2006)

[a] Based on isotopic data from reservoir fluid.
[b] Dominant phase of the reservoir underlying survey area.
[c] Temperature of the reservoir underlying survey area.
[d] Fumarole gas rich in acid magmatic gases (SO_2, HCl, HF) in survey area (Chiodini et al., 1995).
[e] Fumarole chemistry arc/mantle type based on relative N_2, He, and Ar contents (Giggenbach, 1996).
[f] Based on mass balance of systems inflow versus outflow.
[g] Based on chloride:boron ratio of thermal waters (Inguaggiato et al., 2000).

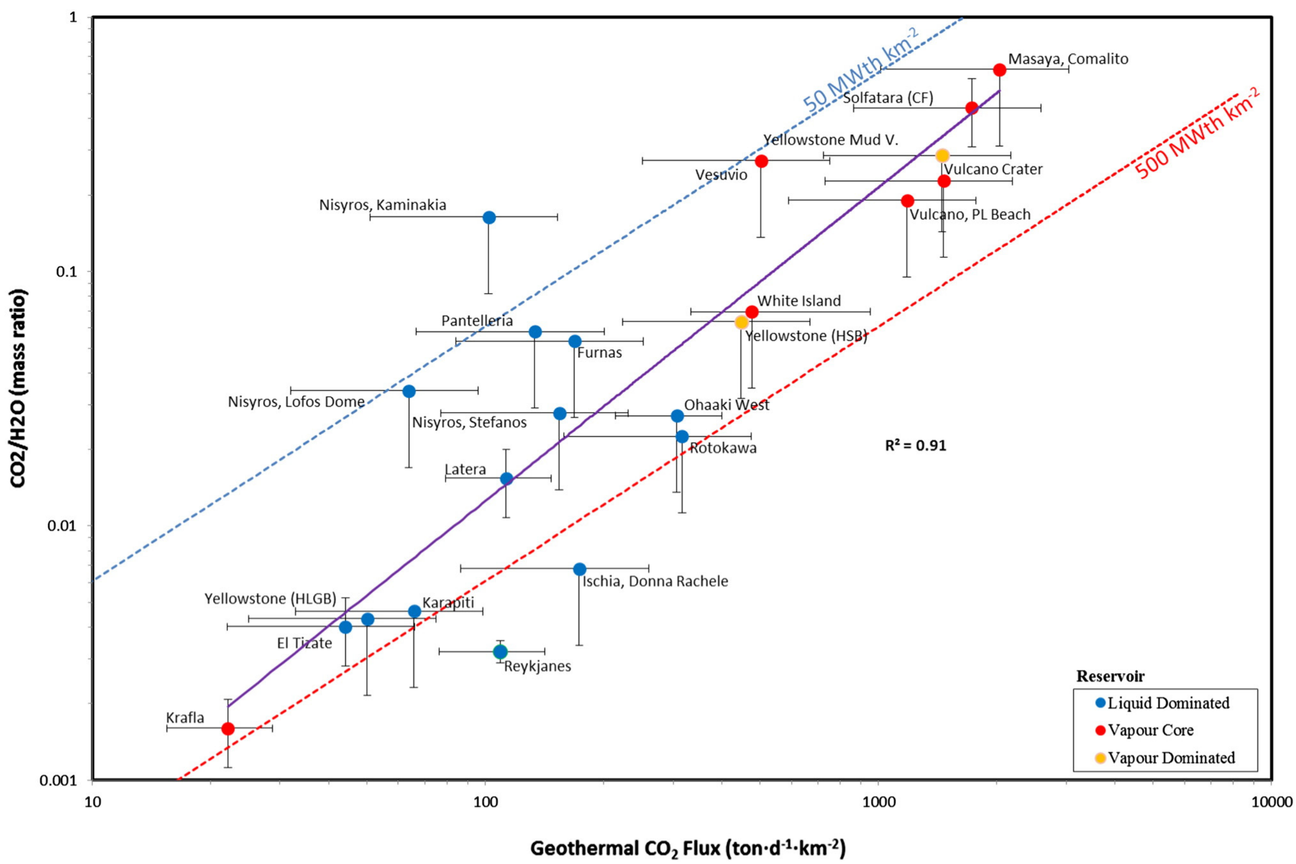

Fig. 1. CO_2/H_2O versus log mean CO_2 flux for hydrothermal systems (data from Table 4). Solid purple line is line of best fit (excludes seawater recharged systems) ($R^2 = 0.91$). Error bars show the uncertainty resulting from fumarole measurements (vertical), or survey methodology (horizontal). (For interpretation of the references to color in this figure legend, the reader is referred to the web version of this article.)

have a >50% probability of exceeding twice the mean background (biogenic) flux (Chiodini et al., 2005). Some surveys were confined to thermal ground with little or no vegetation. In these cases the DDS area was assumed to be where CO_2 fluxes exceeded zero; the biogenic flux was assumed to be negligible (refer Tables 2 and 3). The uncertainty of the CO_2 flux estimate was computed from the simulation results, and found to be a function of CO_2 flux measurement density. The measurement density defined by number of measurements falling in the area contained by circle with radius equal to the range of the CO_2 flux variogram (circle range area (CRA)) (Cardellini et al., 2003). Raw data from recent CO_2 flux surveys at Ohaaki, Rotokawa, White Island (New Zealand) and San Jacinto (Nicaragua) were reprocessed using this approach (refer Tables 2 and 3).

Summary data from a variety of surveyed hydrothermal areas are tabulated (Table 4). The calculated mean CO_2 flux for the various DDS areas is plotted against CO_2/H_2O ratios (from fumarole or deep well gas analysis) for each area on a log–log plot (Fig. 1). For most DDS considered here, the contribution of focused venting from fumaroles inside the DDS has been previously reported or is assumed minor (<10%). Table 4 and Fig. 1 include the contribution of focused venting. Mean CO_2 flux error bars are larger (±50%) than previously used (±30%) (Chiodini et al., 2005), to allow for the added uncertainty in this contribution. There are no hot, neutral chloride springs within the studied DDS areas, so no contribution of deep reservoir liquid outflows to the surface heat flux.

Data points are color coded according to the hydrothermal reservoir type (liquid, vapor dominated, or vapor core: Section 3.1). Because heat flux is simply the product of CO_2 flux and fumarole H_2O/CO_2, straight lines of constant heat flux (50 and 500 MW km^{-1}, assumes steam condensation at 1 bar and 12 °C) can be conveniently represented in Fig. 1. These lines encompass most of the data points. Error bars show the inherent uncertainty in fumarole measurements due to condensation processes (negative vertical bars), and the determination of mean CO_2 flux (horizontal bars)(Chiodini et al., 2005). The rationale for assumptions, uncertainty, and other details of the method are provided in Tables 2 and 3.

3. Results and discussion

3.1. Variations in mean heat flux

The relatively narrow range of heat fluxes for most of the systems plotted here is consistent with previous observations that heat flow for a variety of high temperature, meteorically recharged systems of similar areal extent (i.e. approximate heat flux) fall within a single order of magnitude (Weir, 2009). The range is narrow relative to the range of permeabilities known to exist in hydrothermal reservoirs, which extend over several orders of magnitude (Weir, 2009); if permeability were the primary constraint on system heat output, then we would also expect to observe a range of heat fluxes that span several orders of magnitude, but this is not the case.

The factors limiting heat flux from hydrothermal systems were investigated using a 1-D analytical model of heat and mass transfer for a hypothetical, meteorically recharged, convecting system (Weir, 2009). Input parameters for the model included water infiltration rates, rainfall catchment area and enthalpy of the rising plume, giving system heat flow as output. The relationship between rainfall catchment and heat flow was explored further using 3-D numerical modeling of hydrothermal system up-flow and catchment areas for multiple systems (Dempsey et al., 2012). This study showed heat flows from individual systems are proportional to catchment area, in agreement with the 1-D analytical model (Weir, 2009). The local meteoric recharge source

Table 2
Survey methods and geostatistics.

Location	# Meas.	Survey area[a]	DDS area[b]	Meas. density[c]	Meas. spacing[d]	CRA (km^2)[e]	*n* (CRA)[f]	Range (m)[g]	ESD (± %)[h]	Notes
Nisyros, Kaminakea	~400	–	0.28	~1430	Variable grid (~20 m)	0.322	460	320	4	DDS area from Caliro et al. (2005). CRA, *n*, range and ESD from combined Nisyros DDS areas (Cardellini et al., 2003). The DDS area is defined by Caliro et al. (2005) as having 3 times the mean background flux. This is a slightly more conservative threshold than used by Chiodini et al. (2005) (2× mean background), but would not significantly affect the CO_2 flux estimate. Accordingly, CO_2 flux uncertainty assumed ± 50%.
Vesuvio	636	5.5	0.33	116	–	–	–	–	30	Number of measurements and survey area are reported by Frondini et al. (2004).
Nisyros, Lofos Dome	~700	–	0.40	~1750	Regular grid (~20 m)	0.322	563	320	4	DDS area from Caliro et al. (2005). CRA, n, range and ESD from combined Nisyros DDS areas (Cardellini et al., 2003). The DDS area is defined by Caliro et al. (2005) as having 3 times the mean background flux. This is a slightly more conservative threshold than used by Chiodini et al. (2005) (twice mean background), but would not significantly affect the CO_2 flux estimate. Accordingly, CO_2 flux uncertainty assumed ± 50%.
Pantelleria	–	–	0.06	–	–	–	–	–	30	All data from Chiodini et al. (2005).
Latera	930	11	3.10	86	Semi–regular grid (100x100m)	0.528	45	410	15	Survey results from Chiodini et al. (2007).
Furnas	1362	5.8	4.80	235	Random (50 – 100 m spacing)	0.283	66	300	12	Survey results from Viveiros et al. (2010). Furnas Caldera includes several DDS, with differing variogram ranges. ESD is for the DDS with lowest measurement density so is considered a maximum.
Masaya, Comalito	678	0.01	0.01	94,495	Irregular	–	–	–	30	Number of measurements and survey area from Lewicki et al. (2003). All other data from Chiodini et al. (2005).
Solfatara (CF)	414	1.40	0.83	296	Random	0.348	103	333	9	DDS area is reported by Chiodini et al. (2005), but based on the data set reported by Cardellini et al. (2003). Cardellini et al. (2003) provide the variogram Range and local background flux.
Yellowstone Mud V.	–	–	0.40	–	–	–	–	–	30	Survey results from Chiodini et al. (2005).
Nisyros, Stefanos	~500	–	0.08	~6250	Variable grid (~20 m)	0.322	2010	320	2	DDS area from Caliro et al. (2005). CRA, n, range and ESD from combined Nisyros DDS areas (Cardellini et al., 2003). The DDS area is mostly confined to the Stefanos Crater and is defined by Caliro et al. (2005) as the area having 3 times the mean background flux. This is a slightly more conservative threshold than used by Chiodini et al. (2005) (twice mean background), but would not significantly affect the CO_2 flux estimate.
Vulcano, PL Beach	~100	–	0.02	~5000	–	–	–	–	30	DDS area is reported by Chiodini et al. (2005).
Vulcano Crater	–	–	0.42	–	–	–	–	–	30	DDS area is reported by Chiodini et al. (2005).
White Island	691	0.30	0.30	2303	Semi–regular grid	0.123	284	198	5	Number of measurements, survey area, and grid spacing from Bloomberg et al. (2012). Variogram Range from unpublished data. DDS area determined from SGS probability map (probability ≥ 0.5), where flux exceeds twice the mean biogenic flux (0 g m^{-2} d^{-1}).
Yellowstone HSB	160	0.16	0.16	1032	25–50 m	–	–	–	30	Survey results from Werner et al. (2008b).
El Tizate	299	8.91	1.46	34	Approx. regular grid (100 x 400 m)	0.554	19	420	24	Number of measurements, survey area, grid spacing and variogram range from this study. DDS area determined from SGS probability map (probability ≥ 0.5), where flux exceeds twice the mean biogenic flux (40 g m^{-2} d^{-1}).
Ohaaki West	1654	0.67	0.06	2469	–	0.045	112	120	9	Number of measurements from Rissmann et al. (2012). DDS determined from SGS probability map (probability ≥ 0.5), where flux exceeds twice the mean biogenic flux (30 g m^{-2} d^{-1}).
Yellowstone (HGLB)	109	0.09	0.04	1202	15	–	–	–	30	All data from Lowenstern et al. (2012). Survey a semi-regular grid (see paragraph (17) in Lowenstern et al. (2012)). Proportion of measurements in each grid "above background" (19 g m^{-2} d^{-1}) from paragraph (28). These proportions used to calculate total "above background" DDS area (0.043 km^2) from areas given in paragraph (28). Mean flux from total geothermal flow (22.9 g s^{-1}, from Table 3 of Lowenstern et al. (2012)) and this area. This is a different approach to the other areas where 2× background was used to define the DDS. However 38 g m^{-2} d^{-1} (2× background) is probably too high for the barren acid thermal ground of the upper group (see Fig. 3a, Lowenstern et al. (2012)).

Table 2 (*continued*)

Location	# Meas.	Survey area[a]	DDS area[b]	Meas. density[c]	Meas. spacing[d]	CRA (km^2)[e]	n (CRA)[f]	Range (m)[g]	ESD (± %)[h]	Notes
Krafla	3095	2.50	0.63	1238	grid (25 × 50 m)	–	–	–	30	All CO_2 flux survey data from Dereinda (2008). DDS area and associated mean CO_2 flux was determined using the graphical statistical approach (GSA) (Chiodini et al., 1998; Dereinda, 2008).
Rotokawa	2545	1.40	0.75	1818	Irregular grid: 5–20 m spacing	0.091	165	170	7	DDS area is the sum of 5 DDS sub-areas at Rotokawa (Bloomberg et al., 2012). DDS sub-areas were determined from SGS probability maps (probability ≥ 0.5), where flux exceeded twice the mean biogenic flux (10 g m^{-2} d^{-1}). Range is the average of variogram ranges for the 5 sub-areas.
Karapiti	105	0.35	0.35	300	Approx. regular grid (25–50 m)	–	–	–	30	Survey results from Werner et al. (2004). DDS area was assumed to be the entire survey area. CO_2 flux was determined from total CO_2 flow (Grid Volume tool in Surfer®) and the DDS area (CO_2 flux = CO_2 flow • survey $area^{-1}$).
Ischia, Donna Rachele	336	0.86	0.06	390	Random	0.080	31	160	18	Survey results from Chiodini et al. (2005).
Reykjanes	352	0.23	0.11	1564	Regular Grid (25 × 25 m)	0.053	83	130	11	All data from Fridriksson et al. (2006). ESD (±11%) calculated based on sample density and Variogram Range.

[a] Survey area (km^2): total CO_2 flux survey area.
[b] DDS area (km^2): unless stated otherwise (see Notes column) the diffuse degasing structure area is determined from SGS probability maps (prob. ≥ 0.5) where flux exceeds twice the mean biogenic flux (Chiodini et al., 2005).
[c] Meas. density: CO_2 flux measurements per square km.
[d] Meas. spacing: pattern of measurements.
[e] CRA (km^2): circle range area — circle with radius equal to the range of the CO_2 flux variogram (Cardellini et al., 2003).
[f] n (CRA): number of CO_2 flux measurements inside the CRA (Cardellini et al., 2003).
[g] Range (m): range of the CO_2 flux variogram (Cardellini et al., 2003).
[h] ESD (± %): estimated standard deviation. Assumed to be ± 30% (Chiodini et al., 2005) unless derived from sample density and variogram range (Cardellini et al., 2003, Fig. 9b).

for these systems was determined by isotope analysis (see collation of isotope studies: Dempsey et al., 2012).

Both studies acknowledge that the models do not consider the effect of surface topography, but will be strongly affected by this factor (Weir, 2009; Dempsey et al., 2012). For example, surface topography will affect the direction and magnitude of groundwater flows; all else being equal, hydrothermal systems located in a basin, and coastal systems, would receive higher lateral recharge than equivalent systems located beneath a cone. Accordingly, basinal systems should in general have a greater supply of water to serve as the medium for convective heat flow.

Indeed, the geographic distribution of many of the hydrothermal systems in the Taupo Volcanic Zone (New Zealand) would appear to be constrained by recharge availability, including Karapiti (Wairakei), Rotokawa and Ohaaki from this study. Fig. 2 shows the distribution of these systems overlaid on an elevation model of the area; it is striking that most of the systems fall along the Waikato River (9 out of 13), which is the primary hydrological drainage channel and topographic low for the Taupo graben.

The systems with the two highest heat fluxes are Reykjanes (1048 MW km^{-2}) and Ischia (766 MW km^{-2}). According to the above discussion, a simple explanation is that both systems receive relatively high recharge. Indeed, both systems are predominantly seawater charged (Sveinbjornsdottir et al., 1986; Inguaggiato et al., 2000), so have a potentially unlimited water supply.

At the other extreme, Vesuvio, Italy (55 MW km^{-2}) has one of the lowest heat fluxes. At Vesuvio, heat flux is not limited by reservoir temperature (360 °C, see Table 1), but by topography. The large Vesuvio cone deflects meteoric recharge away from the system in all directions over a wide (>100 km^2) area (Federico et al., 2002). Accordingly, there is probably little meteoric water available to recharge the system and facilitate convective heat flow.

Heat fluxes for DDS at Pantelleria, Italy, and Nisyros, Greece, are very low (<70 MW km^{-2}). Stefanos DDS at Nisyros (166 MW km^{-2}) comprises only a minor proportion of the total DDS area (12%), so is not representative of the heat flux at Nisyros, and the overall heat flux there is very low (Caliro et al., 2005). Pantelleria and Nisyros both have very low rainfall (≤500 mm yr^{-1} precipitation) (Grassi et al., 1995; Drouza et al., 2007), and isotope geochemistry indicates a proportion of seawater in both reservoirs (Parello et al., 2000; Dotsika et al., 2009). The low heat flux observed at Nisyros and Pantelleria demonstrates that seawater recharge does not always equate to high heat flux (cf. Reykjanes). Instead, seawater recharge only provides the potential for high heat flux where other factors are not limiting (i.e. permeability and/or heat source).

The line of best fit (Fig. 1) indicates a general trend toward lower heat flux for vapor core systems and possibly vapor dominated systems. Mud Volcano and Hot Spring Basin (HSB), Yellowstone, plot among the vapor core systems with moderate heat fluxes. However both systems are vapor dominated, rather than vapor core (Werner et al., 2008b). Vapor dominated systems can develop in locations where recharge is limited by low permeability or other factors (White et al., 1971; Allis, 2000). They differ from vapor core systems because they may have a neutral liquid reservoir at depth (beneath the vapor zone) (White et al., 1971).

Vapor core and vapor dominated systems are often associated with high relief terrain (Fournier, 1989; Allis, 2000). For example, Vesuvio and Vulcano are stratovolcanoes. Mud Volcano and Hot Spring Basin (HSB) are located within the relatively high elevation east-central plateau of Yellowstone Park; the vapor dominated nature of these systems was previously attributed to their high elevation (Fournier, 1989). High relief terrain tends to drain liquid water laterally away to lower elevation catchments; higher elevation geothermal areas often exhibit deep water tables and vapor zones. Accordingly, the trend towards lower heat flux for some vapor core and vapor dominated systems may be explained in terms of recharge.

Alternatively, the moderate heat fluxes at White Island and Masaya may be partly an artifact of sampling bias that results in less measurement in the least accessible areas of vapor core systems, where the most focused emissions are expected; both systems have focused

Table 3
Calculation of mean CO_2 flux and CO_2/H_2O: assumptions and uncertainty.

Location	DDS Area[a]	CO_2 flow (diff.)[b]	CO_2 flow (focus)[c]	Total CO_2 flow[d]	Backgr. stat. ($g\ m^{-2}\ d^{-1}$)[e]	Backgr. contr. ($g\ m^{-2}\ d^{-1}$)[f]	Backgr ^{13}C ($g\ m^{-2}\ d^{-1}$)[g]	CO_2 flux[h]	CO_2 flux error (± %)[i]	CO_2/H_2O[j]	CO_2/H_2O error (%)[k]	Notes
Nisyros, Kaminakea	0.28	26	3	28	–	15.0	–	102	50	0.164	−50	Geothermal CO_2 flow, CO_2/H_2O and DDS area are from Caliro et al. (2005). CO_2/H_2O error (−50%) from Chiodini et al. (2005). Weak fumaroles exist inside DDS areas and assumed to contribute an additional ~10% to diffuse emissions. Background flux from Cardellini et al.(2003).
Vesuvio	0.33	151	15	166	7.2	10.9	–	502	50	0.273	−50	Vesuvio geothermal CO_2 flow is reported by Frondini et al. (2004), ESD (±30%) provided by Chiodini et al.(2005) as a reasonable maximum for the expected error. CO_2/H_2O and associated error (−50%) from Chiodini et al. (2005). Background flux from Frondini et al. (2004). Fumaroles exist inside anomalous areas and assumed to contribute an additional ~10% to diffuse emissions (G. Chiodini Pers. Comm., 2014). CO_2 flux uncertainty assumed ±50%.
Nisyros, Lofos Dome	0.40	23	2	26	–	15.0	–	64	50	0.034	−50	Geothermal CO_2 flow, CO_2/H_2O and DDS area are from Caliro et al. (2005). CO_2/H_2O error (−50%) from Chiodini et al. (2005). Weak fumaroles exist inside DDS areas and assumed to contribute an additional ~10% to diffuse emissions. Background flux from Cardellini et al.(2003). CO_2 flux uncertainty assumed ±50%.
Pantelleria	0.06	7	1	8	–	–	–	133	50	0.058	−50	All data from Chiodini et al. (2005). ESD (±30%) provided by Chiodini et al.(2005) as a reasonable maximum for the expected error. CO_2/H_2O and associated error (−50%) from Chiodini et al. (2005). Weak fumaroles exist inside DDS area and assumed contribute an additional ~10% of diffuse emissions. CO_2 flux uncertainty assumed ±50%.
Latera	3.10	350	0	350	13.9	15.7	–	113	30	0.015	±30	Survey results from Chiodini et al. (2007). CO_2/H_2O ratio based on well fluid analysis. error (±30%) is considered reasonable as well analysis is more reliable than fumarole analysis. No fumaroles exist inside anomalous areas. CO_2 flux error assumed to be ESD (±30%).
Furnas	4.80	734	73	807	80.0	34.0	25.0	168	50	0.053	−50	Survey results from Viveiros et al. (2010). CO_2/H_2O is from recent unpublished data that is based on improved fumarolic gas sampling and analytical procedures. CO_2/H_2O error (−50%) from Chiodini et al. (2005). Fumaroles exist inside DDS areas and assumed to contribute an additional ~10% to diffuse emissions. CO_2 flux uncertainty assumed ±50%.
Masaya, Comalito	0.01	19	2	21	–	–	–	2029	50	0.625	−50	All data from Chiodini et al. (2005). Background levels are not discussed by Lewicki et al. (2003), but ^{13}C isotope values from CO_2 in soil, and the generally very high CO_2 flux suggest almost all CO_2 is of magmatic origin. Only small, weak fumaroles exist inside DDS area and assumed to contribute an additional ~10% to diffuse emissions (J. Lewicki Pers. Comm., 2014). CO_2 flux uncertainty assumed ±50%.
Solfatara (CF)	0.83	1100	330	1430	23.9	–	–	1728	50	0.441	−50	Solfatara Geothermal CO_2 flow and DDS area is reported by Chiodini et al. (2005), but based on the data set reported by Cardellini et al. (2003). Cardellini et al. (2003) provide the local background flux. CO_2/H_2O and associated error (−50%) from Chiodini et al. (2005). Fumaroles exist inside DDS area and contribute an additional ~30% to diffuse emissions (Aiuppa et al., 2013). CO_2 flux uncertainty assumed ±50%.
Yellowstone Mud V.	0.40	290	290	580	–	19.0	–	1450	50	0.287	−50	Survey results from Chiodini et al. (2005). CO_2/H_2O and associated error (−50%) from Chiodini et al. (2005). Background flux from Werner et al. (2000). Fumaroles exist inside DDS area and contribute approximately the same flow of CO_2 as diffuse emissions (Werner et al., 2000). CO_2 flux uncertainty assumed ±50%.

Nisyros, Stefanos	0.08	11	1	12	–	15.0	–	154	50	0.028	−50	Geothermal CO_2 flow, CO_2/H_2O and DDS area are from Caliro et al. (2005). CO_2/H_2O error (−50%) from Chiodini et al. (2005). Weak fumaroles exist inside DDS areas and assumed to contribute an additional ~10% to diffuse emissions. Background flux from Cardellini et al.(2003). CO_2 flux uncertainty assumed ±50%.
Vulcano, PL Beach	0.02	19	2	21	–	–	–	1181	50	0.191	−50	Geothermal CO_2 flow and DDS area is reported by Chiodini et al. (2005). CO_2/H_2O and associated error (−50%) from Chiodini et al. (2005). Statistical analysis conducted by Chiodini et al. (1998), but background flux not stated explicitly. Fumaroles exist inside DDS areas and assumed to contribute an additional ~10% to diffuse emissions. CO_2 flux uncertainty assumed ±50%.
Vulcano Crater	0.42	158	449	607	–	–	–	1463	50	0.227	−50	Survey results from Chiodini et al. (2005). CO_2/H_2O and associated error (−50%) from Chiodini et al. (2005). Statistical analysis conducted by Chiodini et al. (1998), but background flux not stated explicitly. Fumaroles exist inside anomalous areas and assumed 10% of diffuse emmissions (G. Chiodini Pers. Comm., 2014). At Vulcano there is significant temporal variation in total CO_2 flow, accordingly, CO_2 flux uncertainty assumed ±50%.
White Island	0.30	110	33	143	–	–	–	475	+100 / –30	0.070	−50	CO_2/H_2O from Bloomberg et al. (2012). CO_2/H_2O error (−50%) from Chiodini et al. (2005). Biological background flux likely to be negligible as survey area is acidic thermal ground and barren of vegetation. Mean flux, and total CO_2 flow were determined from the declustered mean of raw flux values inside the DDS area boundary. Several strong fumaroles exist inside DDS area and assumed to contribute an additional ~30% to diffuse emissions. CO_2 flux uncertainty assumed +100%/−30% to account for the possibility of a larger/smaller contribution from focused fumarole venting.
Yellowstone HSB	0.16	63	6	69	–	19.0	–	447	50	0.064	−50	Survey results from Werner et al. (2008b). CO_2/H_2O and associated error (−50%) from Chiodini et al. (2005). Background flux from Werner et al. (2000). Fumaroles inside DDS assumed to contribute an additional ~10% to diffuse emissions. CO_2 flux uncertainty assumed ±50%.
El Tizate	1.46	64	0	64	20.0	–	–	44	50	0.004	−50	CO_2/H_2O ratio based on deep reservoir CO_2 content at El Tizate, and assuming boiling from 270–100 °C (Harvey et al., 2011). CO_2/H_2O error (±30%) considered reasonable as well discharge analysis is more reliable than fumarole analysis. Mean flux, and total CO_2 flow were determined from the declustered mean of raw flux values (less biogenic flux) inside the DDS area boundary. No fumaroles exist inside anomalous areas so CO_2 flux error assumed to be ESD (±24%).
Ohaaki West	0.06	20	0	20	15.0	–	15.0	307	30	0.027	−50	Background value from Rissmann et al. (2012). CO_2/H_2O from Rissmann (2010). Mean flux, and total CO_2 flow were determined from the declustered mean of raw flux values (less mean biogenic flux) inside the DDS area. No fumaroles exist inside DDS so CO_2 flux error assumed to be ±30%.
Yellowstone (HGLB)	0.04	2	0	2	–	19.0	–	50	50	0.004	−50	All data from Lowenstern et al. (2012). CO_2/H_2O and associated error (−50%) from Chiodini et al. (2005). Fumaroles exist inside DDS areas and assumed to contribute an additional ~10% to diffuse emissions. CO_2 flux uncertainty assumed ±50%.
Krafla	0.63	14	0	14	6.8	–	–	22	30	0.002	±30	All CO_2 flux survey data from Dereinda (2008). CO_2/H_2O ratio based on vapor samples from representative well discharges at Krafla (Arnorsson et al., 2010. CO_2/H_2O error (±30%) considered reasonable as well discharge analysis is more reliable than fumarole analysis. DDS area and associated mean CO_2 flux was determined using the graphical statistical approach (GSA)(Chiodini et al., 1998; Dereinda, 2008). No fumaroles exist inside DDS and CO_2 flux error assumed to be (±30%).

(continued on next page)

Table 3 (*continued*)

Location	DDS Area[a]	CO_2 flow (diff.)[b]	CO_2 flow (focus)[c]	Total CO_2 flow[d]	Backgr. stat. ($g\ m^{-2}\ d^{-1}$)[e]	Backgr. contr. ($g\ m^{-2}\ d^{-1}$)[f]	Backgr ^{13}C ($g\ m^{-2}\ d^{-1}$)[g]	CO_2 flux[h]	CO_2 flux error (± %)[i]	CO_2/H_2O[j]	CO_2/H_2O error (%)[k]	Notes
Rotokawa	0.75	216	22	237	–	–	–	316	50	0.022	−50	CO_2/H_2O ratio and error (−50%) from deep well measurements (Ward et al., 2006; Hunt and Bowyer, 2007). Mean biogenic background estimated to be 5 $g\ m^{-2}\ d^{-1}$ as a large part of DDS is thermal ground with little vegetation. For each DDS sub-area, mean flux, and total CO_2 flow were determined from the declustered mean of raw flux values (less mean biogenic flux). Range is the average of variogram ranges for the 5 sub-areas. Fumaroles exist inside DDS areas and assumed to contribute an additional ~10% to diffuse emissions. CO_2 flux uncertainty assumed ±50%.
Karapiti	0.35	6	17	23	–	5.0	–	66	50	0.005	−50	Survey results from Werner Werner et al. (2004). CO_2/H_2O estimated error (−50%) suggested by Chiodini et al. (2005). CO_2 flux was determined from total CO_2 flow (Grid Volume tool in Surfer®) and the DDS area (CO_2 flux = CO_2 flow · survey area-1). CO_2 flux uncertainty assumed ±50%. Contribution of focused fumarole discharge from Werner et al. (2004).
Ischia, Donna Rachele	0.06	9	1	10	–	28.7	–	173	50	0.007	−50	Survey results from Chiodini et al. (2005). CO_2/H_2O and associated error (−50%) from Chiodini et al. (2005). Background flux from OUTDDS area (Chiodini et al., 2004). Fumaroles exist inside DDS and assumed to contribute an additional ~10% to diffuse emissions. CO_2 flux uncertainty assumed ±50%.
Reykjanes	0.11	12	0	12	4.1	–	–	109	30	0.003	±10	All data from Fridriksson et al. (2006). CO_2/H_2O is based on agreement between gas measurements from deep well discharge and high flow-rate fumaroles, so error is considered to be low (±10%). CO_2 flux uncertainty assumed ±30%.

[a] DDS area (km^2): unless stated otherwise (see Notes column) the diffuse degasing structure (DDS) area is determined from SGS probability maps (prob. ≥ 0.5) where flux exceeds twice the mean biogenic flux (Chiodini et al., 2005).
[b] CO_2 flow (diff.): geothermal CO_2 flow (tons d^{-1}) for the anom. area from soil diffuse flux survey.
[c] CO_2 flow (focus): estimated geothermal CO_2 flow (tons d^{-1}) from fumaroles within the DDS (s).
[d] Total CO_2 flow (ton d^{-1}): CO_2 flow (diff.) + CO_2 flow (focus).
[e] Backgr. stat. ($g\ m^{-2}\ d^{-1}$): biogenic CO_2 flux estimated using statistical method (Chiodini et al., 1998).
[f] Backgr. contr. area ($g\ m^{-2}\ d^{-1}$): biogenic CO_2 flux estimated from a set of measurements in a non-geothermal area (Chiodini et al., 2007).
[g] Backgr ^{13}C ($g\ m^{-2}\ d^{-1}$): biogenic CO_2 flux estimated on the basis of the carbon (^{13}C) isotopic signature (Chiodini et al., 2008).
[h] CO_2 flux (tons $km^{-2}\ d^{-1}$): total CO_2 flow/DDS area.
[i] CO_2 flux error (± %): est. error for CO_2 flux. Assumed to be 30% (Chiodini et al., 2005), unless large CO_2 flow (focus) is probable.
[j] CO_2/H_2O:CO_2/H_2O mass ratio of the rising vapor plume. Determined from fumarole or deep well gas measurements.
[k] CO_2/H_2O error (%); est. error for CO_2/H_2O. Assumed to be −50% (Chiodini et al., 2005) unless based on deep well gas analysis.

Table 4
Compilation of soil diffuse CO_2 flux survey results.

	Area (km^2)[a]	FCO_2 (tons d^{-1})[b]	CO_2 flux (ton d^{-1} km^{-2})[c]	CO_2/H_2O[d]	Steam flux (ton d^{-1} km^{-2})[e]	Heat flux (MW km^{-2})[f]
Nisyros, Kaminakia	0.28	28	102	0.164	621	19
Vesuvio	0.33	166	502	0.273	1837	55
Nisyros, Lofos Dome	0.40	26	64	0.034	1876	56
Pantelleria	0.06	8	133	0.058	2295	69
Latera	3.10	350	113	0.015	7326	70
Furnas	4.80	808	168	0.053	3164	95
Masaya, Comalito	0.01	21	2029	0.625	3247	97
Solfatara (CF)	0.83	1430	1728	0.441	3922	118
Yellowstone Mud V.	0.40	580	1450	0.287	5060	152
Nisyros, Stefanos	0.08	12	154	0.028	5544	166
Vulcano, PL Beach	0.02	21	1181	0.191	6187	186
Vulcano Crater	0.42	607	1463	0.227	6439	193
White Island	0.30	143	475	0.070	6840	205
Yellowstone (HSB)	0.16	69	447	0.064	7035	211
El Tizate	1.46	64	44	0.004	10,963	329
Ohaaki West	0.06	20	307	0.027	11,305	339
Yellowstone (HLGB)	0.04	2	50	0.004	11,579	347
Krafla	0.63	14	22	0.002	13,802	414
Rotokawa	0.75	237	316	0.022	14,061	422
Karapiti	0.35	23	66	0.005	14,220	427
Ischia, Donna Rachele	0.06	10	173	0.007	25,468	764
Reykjanes	0.11	12	109	0.003	33,982	1019
Mean	0.67	211	504	0.1183	8944	262

[a] Area — DDS area where CO_2 flux has ≥50% probability of exceeding twice the mean background (biogenic) flux, except where stated otherwise (refer to *Notes* in Tables 2 and 3 for details).
[b] FCO_2 — flow of hydrothermal CO_2 within DDS (diffuse + focused venting).
[c] CO_2 flux — FCO_2/DDS area.
[d] CO_2/H_2O — mass ratio of the rising vapor plume, determined from fumarole or deep well measurements.
[e] Steam flux — product of CO_2 flux and H_2O/CO_2.
[f] Heat flux — product of the enthalpy of steam at the local boiling temperature less the enthalpy of water at ambient temperature, and steam flux. Note: excluding Latera where heat flux was derived from the enthalpy of liquid water at reservoir temperature (212 °C).

central plumes that were not included in the survey because the areas are inaccessible. At White Island the central plume underlies an acidic crater lake (Werner et al., 2008a). At Masaya, survey measurements were conducted on the flanks of the volcano (Lewicki et al., 2003).

3.2. Geothermal electric power plants and heat flux

The low power density (electrical capacity per unit area of reservoir) of geothermal power plants supplied by vapor dominated reservoirs at the Geysers (USA) and Lardarello (Italy) was noted previously, and attributed to lower recharge relative to other systems where power plants exist (Allis, 2000). Electrical output at these and most other geothermal power plants (both vapor and liquid dominated) is now routinely supported by artificial recharge (injection) of fluids into the productive reservoir (Stefansson, 1997; Kaya et al., 2011).

It is interesting to note the mean electrical capacity of 53 high-temperature geothermal fields (16.2 MW electric km^{-2}) (Wilmarth and Stimac, 2014). Assuming a typical energy conversion efficiency of 0.1 from thermal energy to electric, 16.2 MW electric km^{-2} equates to 162 MW km^{-2} (Ghoniem, 2011; Zarrouk and Moon, 2014). This value is comparable to the mean heat flux for hydrothermal systems determined in this study (198 MW km^{-2}, excluding seawater systems Reykjanes and Ischia). These values are of the same order of magnitude as the global average solar heat flux captured by the Earth's surface water during evaporation (80 MW km^{-2}), then released during condensation (rain) (Trenberth et al., 2009).

Energy fluxes associated with phase changes in water (i.e. liquid to vapor or vice versa) are related to changes in specific enthalpy of the fluid, which allows heat flux (e.g. MW km^{-2}) and water flux (e.g. tons km^{-2} day^{-1}) to be used interchangeably. Further, such changes are relatively insensitive to temperature; the enthalpy change associated with the condensation of steam (100 °C) to ambient liquid water (12 °C) in hydrothermal areas (2624 kJ kg^{-1}), is similar to that associated with the evaporation of Earth's surface waters (~2260 kJ kg^{-1}). Accordingly, the mean heat flux for meteorically recharged hydrothermal systems determined in this study (198 MW km^{-2}) may be a manifestation of the available incoming solar energy flux, the ultimate driver of the hydrological cycle.

3.3. Variations in CO_2 flux and CO_2/H_2O

In order to determine the cause of variations in CO_2 flux and CO_2/H_2O, we have considered the distribution of flux measurements (Fig. 1) in terms of the reservoir dominant phase and geological setting of the individual systems (Table 1). With the notable exception of Krafla, vapor core systems (red markers in Fig. 1) all plot with high CO_2 fluxes and CO_2/H_2O ratios. The high CO_2 flux results from a degassing magma at depth, where no deep liquid reservoir is present to remove CO_2 during ascent. This contrasts with liquid dominated systems, where a greater proportion of the ascending CO_2 is dissolved in the liquid as HCO_3^-. The HCO_3^- may subsequently exit the system via lateral outflow, or be precipitated in the reservoir as calcite (Giggenbach, 1981). Vapor dominated systems at Yellowstone (Mud Volcano and Hot Spring Basin) also have high CO_2 flux, consistent with a deep, small liquid reservoir that has limited capacity to remove CO_2.

Krafla, despite being a vapor core system, has low CO_2 fluxes and CO_2/H_2O because of its position in newly formed basalt crust; Icelandic magmas are deeply sourced and depleted in volatiles, including CO_2. Similarly, the low CO_2/H_2O of Karapiti (Wairakei) relative to Ohaaki and Rotokawa was previously attributed to the depth of the degassing magma, and the associated depletion of magmatic volatiles (Giggenbach, 1995). This would also explain the low CO_2 flux of Karapiti relative to Ohaaki and Rotokawa.

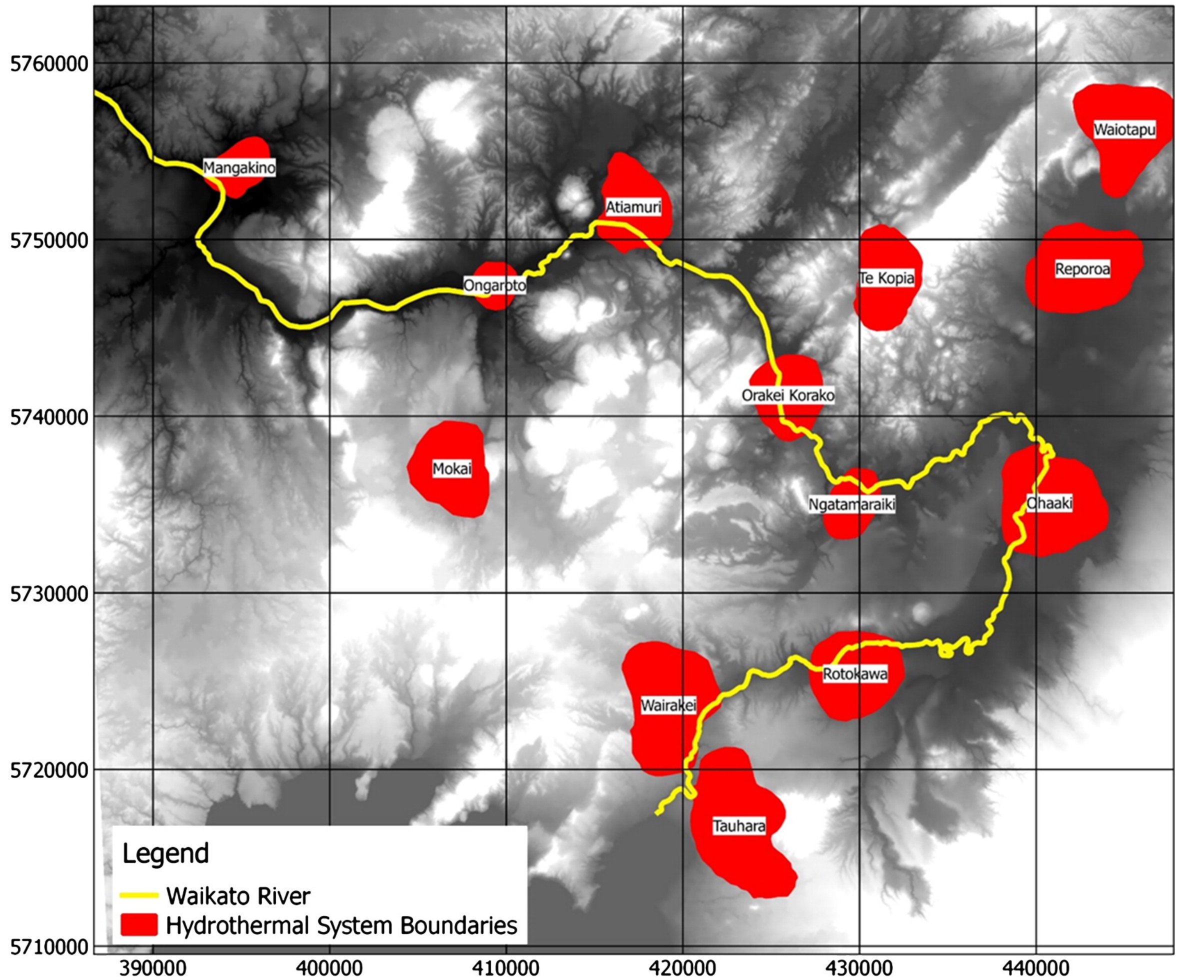

Fig. 2. Location of hydrothermal fields (red areas) in the Taupo Volcanic Zone overlaid on a satellite digital terrain model (WGS84). Darker shading indicates lower elevation. Field boundaries are based on shallow electrical resistivity data (Bibby et al., 1995). (For interpretation of the references to color in this figure legend, the reader is referred to the web version of this article.)

4. Conclusions

Our results show that variations in the CO_2 flux, CO_2/H_2O, and associated heat flux seen in the systems examined here may be explained in terms of the specific geological and hydrological setting of the systems. Our results indicate that recharge availability exerts a strong control over the location of hydrothermal systems, and in some cases may constrain the heat flux from hydrothermal systems (i.e. vapor systems). Recharge is in turn governed by permeability, structure, rainfall, topography, and possibly proximity to an unlimited supply of water such as the ocean. The relationship between recharge and convective heat flux interpreted by this study is consistent with recent numerical modeling that relates system heat output to rainfall catchment area.

This finding has implications for the development of hydrothermal electricity, currently slowed by the economic risks of exploration. We identify recharge availability as an important factor in resource prospectively, and the utility of the CO_2 flux survey technique for geothermal resource evaluation.

Acknowledgments

We would like to acknowledge the Faculty of Engineering at Auckland University, and GNS Science, New Zealand for providing research funding. We would like to thank Ram Power and Polaris Energy Nicaragua S.A. for allowing publication of survey results at El Tizate. All data necessary to understand, evaluate, replicate, and build upon the reported research are provided in Tables 2 and 3.

References

Aiuppa, A., Tamburello, G., Napoli, R., Cardellini, C., Chiodini, G., Giudice, G., Grassa, F., Pedone, M., 2013. First observations of the fumarolic gas output from a restless caldera: implications for the current period of unrest (2005–2013) at Campi Flegrei. Geochem. Geophys. Geosyst. 14, 4153–4169.

Allis, R., 2000. Insights on the formation of vapor-dominated geothermal systems. Proc. World Geoth. Congr.Kyushu - Tohoku, Japan

Arnorsson, S., Angcoy, E., Bjarnason, J.Ö., Giroud, N., Gunnarsson, I., Kaasalainen, H., Karingithi, C., Stefánsson, A., 2010. Gas chemistry of volcanic geothermal systems. Proc. World Geoth. Congr. Bali, Indonesia.

Bibby, H.M., Caldwell, T.G., Davey, F.J., Webb, T.H., 1995. Geophysical evidence on the structure of the Taupo volcanic zone and its hydrothermal circulation. J. Volcanol. Geotherm. Res. 68, 29–58.

Bird, R.B., Stewart, W.E., Lightfoot, E.N., 1960. Trans. Phenom. vol. 2. Wiley, New York.

Bloomberg, S., Rissmann, C., Mazot, A., Oze, C., Horton, T., Gravley, D., Kennedy, B., Werner, C., Christenson, B., Pawson, J., 2012. Soil gas flux exploration at the Rotokawa geothermal field and White Island, New Zealand. Proceedings, 36th Workshop on Geothermal Reservoir Engineering. Stanford, California, USA.

Bolognesi, L., D'Amore, F., 1993. Isotopic variation of the hydrothermal system on Vulcano Island, Italy. Geochim. Cosmochim. Acta 57, 2069–2082.

Brombach, T., Hunziker, J.C., Chiodini, G., Cardellini, C., Marini, L., 2001. Soil diffuse degassing and thermal energy fluxes from the southern Lakki plain, Nisyros (Greece). Geophys. Res. Lett. 28, 69–72.

Brombach, T., Caliro, S., Chiodini, G., Fiebig, J., Hunziker, J.C., Raco, B., 2003. Geochemical evidence for mixing of magmatic fluids with seawater, Nisyros hydrothermal system, Greece. Bull. Volcanol. 65, 505–516.

Caliro, S., Chiodini, G., Galluzzo, D., Granieri, D., La Rocca, M., Saccorotti, G., Ventura, G., 2005. Recent activity of Nisyros volcano (Greece) inferred from structural, geochemical and seismological data. Bull. Volcanol. 67, 358–369.

Cardellini, C., Chiodini, G., Frondini, F., 2003. Application of stochastic simulation to CO_2 flux from soil: mapping and quantification of gas release. J. Geophys. Res. Solid Earth 108.

Chamorro, C.R., Mondéjar, M.E., Ramos, R., Segovia, J.J., Martín, M.C., Villamañán, M.A., 2012. World geothermal power production status: energy, environmental and economic study of high enthalpy technologies. Energy 42, 10–18.

Chiodini, G., Cioni, R., Marini, L., Panichi, C., 1995. Origin of the fumarolic fluids of Vulcano Island, Italy and implications for volcanic surveillance. Bull. Volcanol. 57, 99–110.

Chiodini, G., Frondini, F., Raco, B., 1996. Diffuse emission of CO_2 from the Fossa crater, Vulcano Island (Italy). Bull. Volcanol. 58, 41–50.

Chiodini, G., Cioni, R., Guidi, M., Raco, B., Marini, L., 1998. Soil CO_2 flux measurements in volcanic and geothermal areas. Appl. Geochem. 13, 543–552.

Chiodini, G., Frondini, F., Cardellini, C., Granieri, D., Marini, L., Ventura, G., 2001a. CO_2 degassing and energy release at Solfatara volcano, Campi Flegrei, Italy. J. Geophys. Res. Solid Earth 106, 16213–16221.

Chiodini, G., Marini, L., Russo, M., 2001b. Geochemical evidence for the existence of high-temperature hydrothermal brines at Vesuvio volcano, Italy. Geochim. Cosmochim. Acta 65, 2129–2147.

Chiodini, G., Avino, R., Brombach, T., Caliro, S., Cardellini, C., De Vita, S., Frondini, F., Granirei, D., Marotta, E., Ventura, G., 2004. Fumarolic and diffuse soil degassing west of Mount Epomeo, Ischia, Italy. J. Volcanol. Geotherm. Res. 133, 291–309.

Chiodini, G., Granieri, D., Avino, R., Caliro, S., Costa, A., Werner, C., 2005. Carbon dioxide diffuse degassing and estimation of heat release from volcanic and hydrothermal systems. J. Geophys. Res. Solid Earth 110.

Chiodini, G., Baldini, A., Barberi, F., Carapezza, M., Cardellini, C., Frondini, F., Granieri, D., Ranaldi, M., 2007. Carbon dioxide degassing at Latera caldera (Italy): evidence of geothermal reservoir and evaluation of its potential energy. J. Geophys. Res. Solid Earth 112.

Chiodini, G., Caliro, S., Cardellini, C., Avino, R., Granieri, D., Schmidt, A., 2008. Carbon isotopic composition of soil CO_2 efflux, a powerful method to discriminate different sources feeding soil CO_2 degassing in volcanic–hydrothermal areas. Earth Planet. Sci. Lett. 274, 372–379.

Cruz, J.V., Coutinho, R.M., Carvalho, M.R., Oskarsson, N., Gislason, S.R., 1999. Chemistry of waters from Furnas volcano, São Miguel, Azores: fluxes of volcanic carbon dioxide and leached material. J. Volcanol. Geotherm. Res. 92, 151–167.

Dempsey, D., Simmons, S., Archer, R., Rowland, J., 2012. Delineation of catchment zones of geothermal systems in large-scale rifted settings. J. Geophys. Res. Solid Earth (1978–2012) 117.

Dereinda, F.H., 2008. CO_2 Emissions from the Krafla Geothermal Area, Iceland, United Nations University Geothermal Training Programme, Reports 2008.

Dotsika, E., Poutoukis, D., Michelot, J., Raco, B., 2009. Natural tracers for identifying the origin of the thermal fluids emerging along the Aegean volcanic arc (Greece): evidence of arc-type magmatic water (ATMW) participation. J. Volcanol. Geotherm. Res. 179, 19–32.

Drouza, S., Georgoulias, F., Moustakas, N., 2007. Investigation of soils developed on volcanic materials in Nisyros Island, Greece. Catena 70, 340–349.

Duchi, V., Campana, M.E., Minissale, A., Thompson, M., 1994. Geochemistry of thermal fluids on the volcanic isle of Pantelleria, southern Italy. Appl. Geochem. 9, 147–160.

Federico, C., Aiuppa, A., Allard, P., Bellomo, S., Jean-Baptiste, P., Parello, F., Valenza, M., 2002. Magma-derived gas influx and water–rock interactions in the volcanic aquifer of Mt. Vesuvius, Italy. Geochim. Cosmochim. Acta 66, 963–981.

Fournier, R.O., 1989. Geochemistry and dynamics of the Yellowstone National Park hydrothermal system. Annu. Rev. Earth Planet. Sci. 17, 13.

Fridriksson, T., Kristjánsson, B.R., Ármannsson, H., Margrétardóttir, E., Ólafsdóttir, S., Chiodini, G., 2006. CO_2 emissions and heat flow through soil, fumaroles, and steam heated mud pools at the Reykjanes geothermal area, SW Iceland. Appl. Geochem. 21, 1551–1569.

Frondini, F., Chiodini, G., Caliro, S., Cardellini, C., Granieri, D., Ventura, G., 2004. Diffuse CO_2 degassing at Vesuvio, Italy. Bull. Volcanol. 66, 642–651.

Ghoniem, A.F., 2011. Needs, resources and climate change: clean and efficient conversion technologies. Prog. Energy Combust. Sci. 37, 15–51.

Gianelli, G., Grassi, S., 2001. Water–rock interaction in the active geothermal system of Pantelleria, Italy. Chem. Geol. 181, 113–130.

Giggenbach, W.F., 1981. Geothermal mineral equilibria. Geochim. Cosmochim. Acta 45, 393–410.

Giggenbach, W., 1987. Redox processes governing the chemistry of fumarolic gas discharges from White Island, New Zealand. Appl. Geochem. 2, 143–161.

Giggenbach, W.F., 1995. Variations in the chemical and isotopic composition of fluids discharged from the Taupo Volcanic Zone, New Zealand. J. Volcanol. Geotherm. Res. 68, 89–116.

Giggenbach, W., 1996. Chemical composition of volcanic gases. Monitoring and Mitigation of Volcano Hazards. Springer, pp. 221–256.

Giggenbach, W., Shinohara, H., Kusakabe, M., Ohba, T., 2003. Formation of acid volcanic brines through interaction of magmatic gases, seawater, and rock within the White Island volcanic–hydrothermal system, New Zealand. Soc. Econ. Geol. Spec. Publ. 10, 19–40.

Glover, R.B., Mroczek, E.K., 2009. Chemical changes in natural features and well discharges in response to production at Wairakei, New Zealand. Geothermics 38, 117–133.

Grassi, S., Squarci, P., D'Amore, F., Mussi, M., 1995. Circulation of Thermal Waters on Pantelleria Island (Sicily Channel, Italy). Proc. World Geoth. Congr.Florence, Italy

Harvey, M.C., White, P.J., MacKenzie, K.M., Lovelock, B.G., 2011. Results from a Soil CO_2 Flux and Shallow Temperature Survey at the San Jacinto–Tizate Geothermal Power Project, Nicaragua. Proceedings, New Zealand Geothermal Workshop, November 2011. Auckland, New Zealand.

Hedenquist, J.W., Simmons, S.F., Giggenbach, W.F., Eldridge, C.S., 1993. White Island, New Zealand, volcanic–hydrothermal system represents the geochemical environment of high-sulfidation Cu and Au ore deposition. Geology 21, 731–734.

Henley, R., Ellis, A.J., 1983. Geothermal systems ancient and modern: a geochemical review. Earth-Sci. Rev. 19, 1–50.

Hernández, P.A., Pérez, N.M., Fridriksson, T., Egbert, J., Ilyinskaya, E., Thárhallsson, A., Ívarsson, G., Gíslason, G., Gunnarsson, I., Jónsson, B., 2012. Diffuse volcanic degassing and thermal energy release from Hengill volcanic system, Iceland. Bull. Volcanol. 74, 2435–2448.

Hochstein, M.P., Bromley, C.J., 2005. Measurement of heat flux from steaming ground. Geothermics 34, 131–158.

Hochstein, M.P., Sudarman, S., 2008. History of geothermal exploration in Indonesia from 1970 to 2000. Geothermics 37, 220–266.

Houghton, B., Nairn, I., 1991. The 1976–1982 Strombolian and phreatomagmatic eruptions of White Island, New Zealand: eruptive and depositional mechanisms at a 'wet' volcano. Bull. Volcanol. 54, 25–49.

Hunt, T., Bowyer, D., 2007. Reinjection and gravity changes at Rotokawa geothermal field, New Zealand. Geothermics 36, 421–435.

Inguaggiato, S., Pecoraino, G., D'Amore, F., 2000. Chemical and isotopical characterisation of fluid manifestations of Ischia Island (Italy). J. Volcanol. Geotherm. Res. 99, 151–178.

Kaya, E., Zarrouk, S.J., O'Sullivan, M.J., 2011. Reinjection in geothermal fields: a review of worldwide experience. Renew. Sust. Energ. Rev. 15, 47–68.

Lewicki, J., Connor, C., St-Amand, K., Stix, J., Spinner, W., 2003. Self-potential, soil CO_2 flux, and temperature on Masaya volcano, Nicaragua. Geophys. Res. Lett. 30.

Lewicki, J.L., Bergfeld, D., Cardellini, C., Chiodini, G., Granieri, D., Varley, N., Werner, C., 2005. Comparative soil CO_2 flux measurements and geostatistical estimation methods on Masaya volcano, Nicaragua. Bull. Volcanol. 68 (1), 76–90.

Lowenstern, J., Bergfeld, D., Evans, W., Hurwitz, S., 2012. Generation and evolution of hydrothermal fluids at Yellowstone: insights from the Heart Lake Geyser Basin. Geochem. Geophys. Geosyst. 13.

MacNeil, R.E., 2006. Geophysical Investigations and Groundwater Modelling of the Hydrologic Conditions at Masaya Caldera, Nicaragua (M.S. thesis, Univ. South Florida) http://scholarcommons.usf.edu/etd/3838/.

Nielsen, G., Maack, R., Gudmundsson, A., Gunnarsson, G.I., 2000. Completion of Krafla Geothermal Power Plant, Proceedings, World Geotherm. Congr. 2000.

Ostapenko, S.V., Spektor, S.V., Netesov, Y.P., 1998. San Jacinto–Tizate geothermal field, Nicaragua: exploration and conceptual model. Geothermics 27, 361–378.

Panichi, C., Volpi, G., 1999. Hydrogen, oxygen and carbon isotope ratios of Solfatara fumaroles (Phlegrean Fields, Italy): further insight into source processes. J. Volcanol. Geotherm. Res. 91, 321–328.

Parello, F., Allard, P., D'Alessandro, W., Federico, C., Jean-Baptiste, P., Catani, O., 2000. Isotope geochemistry of Pantelleria volcanic fluids, Sicily Channel rift: a mantle volatile end-member for volcanism in southern Europe. Earth Planet. Sci. Lett. 180, 325–339.

Rissmann, C. (2010), Using Surface Methods to Understand the Ohaaki Field, Taupo Volcanic Zone, New Zealand, Unpublished doctoral dissertation, University of Canterbury, Christchurch, New Zealand, 1-176.

Rissmann, C., Christenson, B., Werner, C., Leybourne, M., Cole, J., Gravley, D., 2012. Surface heat flow and CO_2 emissions within the Ohaaki hydrothermal field, Taupo Volcanic Zone, New Zealand. Appl. Geochem. 27, 223–239.

Rye, R.O., Truesdell, A.H., 2007. The question of recharge to the deep thermal reservoir underlying the geysers and hot springs of Yellowstone National Park. U. S. Geol. Surv. Prof. Pap. 1717.

Sheppard, D., Truesdell, A., Janik, C., 1992. Geothermal gas compositions in Yellowstone National Park, USA. J. Volcanol. Geotherm. Res. 51, 79–93.

Stefansson, V., 1997. Geothermal reinjection experience. Geothermics 26, 99–139.

Sveinbjornsdottir, A., Coleman, M., Yardley, B., 1986. Origin and history of hydrothermal fluids of the Reykjanes and Krafla geothermal fields, Iceland. Contrib. Mineral. Petrol. 94, 99–109.

Trenberth, K.E., Fasullo, J.T., Kiehl, J., 2009. Earth's global energy budget. Bull. Am. Meteorol. Soc. 90.

Viveiros, F., Cardellini, C., Ferreira, T., Caliro, S., Chiodini, G., Silva, C., 2010. Soil CO_2 emissions at Furnas volcano, São Miguel Island, Azores archipelago: volcano monitoring perspectives, geomorphologic studies, and land use planning application. J. Geophys. Res. Solid Earth 115.

Ward, K., Brown, K., Webster-Brown, J., 2006. Mineral Precipitation in the Rotokawa Geothermal Power Station, New Zealand, Proceedings, 28th New Zealand Geothermal Workshop, November 2006. Auckland, New Zealand.

Weir, G.J., 2009. A mathematical model of rainfall-controlled geothermal fields. Transp. Porous Media 77, 323–334.

Werner, C.A., Hochstein, M.P., Bromley, C.J., December 2004. CO_2-flux of steaming ground at Karapiti, Wairakei. Proceedings, 26th New Zealand Geothermal Workshop.

Werner, C., Brantley, S., 2003. CO_2 emissions from the Yellowstone volcanic system. Geochem. Geophys. Geosyst. 4.

Werner, C., Brantley, S., Boomer, K., 2000. CO_2 emissions related to the Yellowstone volcanic system: 2. Statistical sampling, total degassing, and transport mechanisms. J. Geophys. Res. Solid Earth 105, 10831–10846.

Werner, C., Chiodini, G., Granieri, D., Caliro, S., Avino, R., Russo, M., 2006. Eddy covariance measurements of hydrothermal heat flux at Solfatara volcano, Italy. Earth Planet. Sci. Lett. 244, 72–82.

Werner, C., Hurst, T., Scott, B., Sherburn, S., Christenson, B., Britten, K., Cole-Baker, J., Mullan, B., 2008a. Variability of passive gas emissions, seismicity, and deformation during crater lake growth at White Island Volcano, New Zealand, 2002–2006. J. Geophys. Res. Solid Earth 113.

Werner, C., Hurwitz, S., Evans, W., Lowenstern, J., Bergfeld, D., Heasler, H., Jaworowski, C., Hunt, A., 2008b. Volatile emissions and gas geochemistry of Hot Spring Basin, Yellowstone National Park, USA. J. Volcanol. Geotherm. Res. 178, 751–762.
White, D.E., Muffler, L.J.P., Truesdell, A.H., 1971. Vapor-dominated hydrothermal systems compared with hot-water systems. Econ. Geol. 66, 75–97.
Wilmarth, M., Stimac, J., 2014. Worldwide Power Density Review. 39th Workshop on Geothermal Reservoir Engineering, Proceedings, February 2014. Stanford, California, USA.
Zarrouk, S.J., Moon, H., 2014. Efficiency of geothermal power plants: a worldwide review. Geothermics 51, 142–153.